REPRINTED FROM:

# TURBULENCE AND CHAOTIC PHENOMENA IN FLUIDS

*Proceedings of the International Symposium on Turbulence and Chaotic Phenomena in Fluids, held in Kyoto, Japan, 5-10 September, 1983 sponsored by The International Union of Theoretical and Applied Mechanics*

Edited by
Tomomasa TATSUMI
*Department of Physics*
*Faculty of Science*
*University of Kyoto*
*Kyoto, Japan*


1984

NORTH-HOLLAND
AMSTERDAM • NEW YORK • OXFORD

TURBULENCE AND CHAOTIC PHENOMENA IN FLUIDS
T. Tatsumi (editor)
Elsevier Science Publishers B.V. (North-Holland)
© IUTAM, 1984


# Transition and Mixing in Impulsively Started Jets and Vortex Rings

by

Brian J. Cantwell and Gary A. Allen, Jr.
Department of Aeronautics and Astronautics
Stanford University
Stanford, California
U.S.A.

A new method is used to analyze transition in implusively started jets and vortex rings. The method uses similarity variables to reduce the equations for unsteady particle paths to a quasi–autonomous system with the Reynolds number as a parameter. The flow pattern is represented in terms of the phase portrait of this system and the structure of the flow is defined by its critical points. Flow transition is examined in terms of bifurcations in the topology of the phase portrait which occur as the Reynolds number is increased. There is no assumption that the flow is parallel or that it is subjected to small disturbances. The method of analysis, though straightforward, is new and lies outside the usual small disturbance theory used to determine the stability of various profile shapes.

## I. Introduction

We are considering viscous, incompressible, axisymmetric flows produced by a time dependent point source of momentum of strength $F(t)$ (force/density, units $L^4/T^2$) acting on an infinite fluid. Three complimentary flows have been studied; a vortex ring produced by an impulse force, a round jet produced by a step force which turns on at $t = 0$ and remains on for all time, and a ramp jet produced by a force that increases linearly with time. In the case of the round jet the Reynolds number is independent of time and the reduced particle path equations are strictly autonomous. The vortex ring has a Reynolds number which decreases like $t^{-1/2}$ and its compliment, the ramp jet, has a Reynolds number which increase like $t^{1/2}$. In the latter two cases the particle path equations reduce to a quasi–autonomous system and the phase portrait varies with time.

The governing equations in spherical polar coordinates are given by

$$u = \frac{1}{r^2 \sin\theta}\frac{\partial \psi}{\partial \theta} \qquad v = -\frac{1}{r \sin\theta}\frac{\partial \psi}{\partial r} \tag{1}$$

$$rw = \frac{\partial}{\partial r}(rv) - \frac{\partial u}{\partial \theta} \tag{2}$$

$$\frac{\partial}{\partial t}(rw) + \frac{\partial}{\partial r}(ruw) + \frac{\partial}{\partial \theta}(vw) = \nu\left\{\frac{1}{r}\frac{\partial}{\partial \theta}\left(\frac{1}{\sin\theta}\frac{\partial}{\partial \theta}(w \sin\theta)\right) + \frac{\partial^2}{\partial r^2}(rw)\right\} \tag{3}$$

where $u$ and $v$ are the radial ($r$) and tangential ($\theta$) velocities in spherical polar coordinates; $w$ is the vorticity and $\psi$ is the stokes stream function. In addition these flows satisfy the integral constraint

$$\frac{2}{3}\frac{I}{\rho} = \int_0^{\pi}\int_0^{\infty}(u\cos\theta - v\sin\theta)2\pi r^2\sin\theta dr d\theta \tag{4}$$

where $I/\rho = \int_0^t F(t)dt$ is the total impulse applied to the fluid.

## II. Linearized Solutions

Much of the structure of the flow is found to be contained in the creeping limit $Re \to 0$. See reference 1. In this case the nonlinear convective terms are small and equation (3) reduces to the linear vorticity diffusion equation. We search for similarity solutions of the form

$$\psi = M\nu^{-1/2}t^{n+1/2}G(\xi,\theta) \quad ; \qquad \xi = \frac{r}{\sqrt{\nu t}} \tag{5}$$

where $M$ is a governing parameter and $\nu$ is the kinematic viscosity.

Solutions are:

i) Vortex ring:

$$F(t) = (I/\rho)\varsigma(t) \quad ; \qquad M = I/\rho\,(units \quad L^4/T)$$
$$n = -1\,; \qquad Re = (I/\rho)^{1/2}/\nu t^{1/2}\,; \qquad \varsigma(t) = delta\ function$$

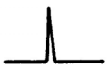

$$G(\xi,\theta) = \frac{1}{4\pi}\sin^2\theta\left\{\frac{1}{\xi}erf(\frac{\xi}{2}) - \frac{1}{\sqrt{\pi}}e^{-\xi^2/4}\right\} \tag{6}$$

ii) Round jet:

$$F(t) = (J/\rho)u(t) \quad ; \qquad M = J/\rho\,(units \quad L^4/T^2)$$
$$n = 0\,, \qquad Re = (J/\rho)^{1/2}/\nu\,; \qquad u(t) = step\ function$$

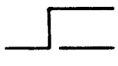

$$G(\xi,\theta) = \frac{1}{16\pi}\sin^2\theta\left\{2\xi - \frac{4}{\sqrt{\pi}}e^{-\xi^2/4} - (2\xi - \frac{4}{\xi})erf(\frac{\xi}{2})\right\} \tag{7}$$

iii) Ramp jet:

$$F(t) = (K/\rho)t \quad ; \qquad M = K/\rho\,(units \quad (L^4/T^3)$$
$$n = 1\,, \qquad Re = (K/\rho)^{1/2}t^{1/2}/\nu$$

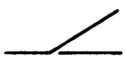

$$G(\xi,\theta)=\frac{1}{16\pi}\sin^2\theta\left\{(\frac{\xi^3}{2}+2\xi)(1-erf(\frac{\xi}{2}))+\frac{2}{\xi}erf(\frac{\xi}{2})-\frac{1}{\sqrt{\pi}}(2+\xi^2)e^{-\xi^2/4}\right\} \tag{8}$$

where $Re$ denotes the Reynolds number of the flow in question.

## III. Particle Paths

The analysis is focused on the equations for particle paths which, in spherical polar coodinates, are:

$$\frac{dr}{dt}=u(r,\theta,t) \quad ; \quad \frac{d\theta}{dt}=\frac{v(r,\theta,t)}{r} \tag{9}$$

In terms of similarity variables;

$$\frac{d\xi}{d\tau}=Re^2U(\xi,\theta)-\frac{\xi}{2} \quad ; \quad \frac{d\theta}{d\tau}=Re^2\frac{V(\xi,\theta)}{\xi} \quad ; \quad \tau=ln(t) \tag{10}$$

where

$$U=\frac{1}{\xi^2\sin\theta}\frac{\partial G}{\partial\theta} \quad ; \quad V=-\frac{1}{\xi\sin\theta}\frac{\partial G}{\partial\xi} \tag{11}$$

and

$$Re=\frac{M^{1/2}t^{n/2}}{\nu} \qquad n=\begin{cases}-1 & vortex\,ring\\ 0 & round\,jet\\ 1 & ramp\,jet\end{cases} \tag{12}$$

Critical points $(\xi_c,\theta_c)$ occur where

$$Re^2=\frac{\xi_c}{2U(\xi_c,\theta_c)} \quad ; \quad V(\xi_c,\theta_c)=0 \tag{13}$$

near a critical point $(\xi_c,\theta_c)$

$$\begin{bmatrix}\frac{d\xi}{d\tau}\\ \frac{d\theta}{d\tau}\end{bmatrix}=\begin{bmatrix}a & b\\ c & d\end{bmatrix}\begin{bmatrix}\xi-\xi_c\\ \theta-\theta_c\end{bmatrix} \tag{14}$$

The character of the point is determined by $p$ and $q$ where

$$p=-(a+d) \quad ; \quad q=ad-bc \tag{15}$$

In general the coordinates of the critical points $(\xi_c,\theta_c)$ and the associated values of $p$ and $q$ are functions of the Reynolds number (or time) and the possibility of bifurcation follows.

For the class of flows considered, transition is found to consist of a sequence of critical Reynolds numbers at which bifurcations in the phase portrait of the particle path equations

(hereafter called the entrainment diagram) occur. The linear solutions given by (6), (7) and (8) are found to contain remarkably complex dynamics. When these solutions are examined at Reynolds numbers which lie outside of their region of validity two critical Reynolds numbers and three distinct states of motion are found. Figure 1 depicts the $(p, q)$ trajectories for the three flows studied. Below the first critical Reynolds number, $Re_1$, the entrainment diagram (Figure 2) consists of a single stable node on the flow axis. As the Reynolds number is increased above $Re_1$ the stable node splits to form an on–axis saddle and an off–axis node. As the Reynolds number is further increased above the second critical Reynolds number, $Re_2$, the off–axis node becomes a stable focus. Of particular significance is the time dependence of the Reynolds number in each case and the contrasting physical interpretations of the respective entrainment diagrams. In the case of the round jet $Re_1$ defines the initiation of a new, intermediate, state of motion and $Re_2$ defines the critical Reynolds number for the onset of a starting vortex. In the case of a vortex ring the entrainment diagram describes the late stages of decay and $Re_2$ defines a dimensionless time at which the ability of the flow to roll up a fluid interface terminates. In the case of the ramp jet the entrainment diagram describes transition in the early time history of the flow and $Re_2$ defines a dimensionless time at which a starting vortex begins.

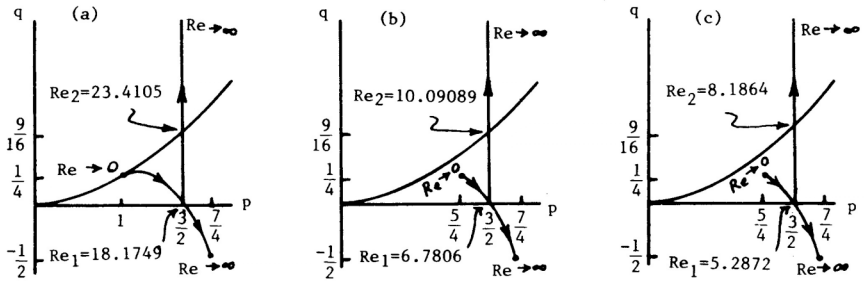


Figure 1. Trajectories $p(Re)$, $q(Re)$ of the critical points of: a) the vortex ring, b) the round jet, c) the ramp jet.

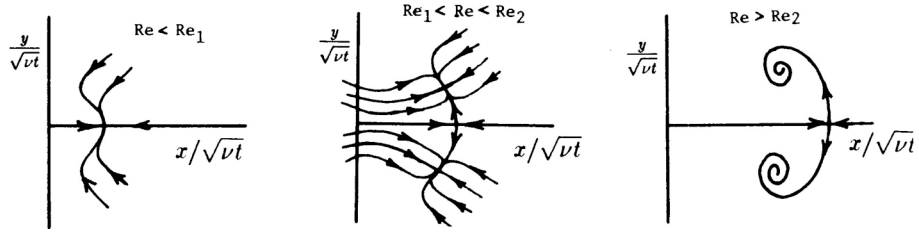


Figure 2. Entrainment diagrams showing three states of motion for jets and vortex rings.

## IV. Universality of Structure

We have seen that the flow topology can be described in terms of its entrainment diagram and that bifurcations at various critical Reynolds numbers are analyzed using the trajectory of the critical points in the $(p, q)$ plane. We may ask; what minimum information is required to construct this trajectory?

To examine this question we apply the continuity equation to the particle path equations. In spherical polar coordinates continuity gives

$$2U + \xi\frac{\partial U}{\partial \xi} + \frac{\cos\theta}{\sin\theta}V + \frac{\partial V}{\partial \theta} = 0 \tag{16}$$

Near a critical point $(\xi_c, \theta_c)$

$$\begin{aligned} Re^2 U &= \frac{\xi}{2} + a(\xi - \xi_c) + b(\theta - \theta_c) \\ Re^2 V &= c\xi(\xi - \xi_c) + d\xi(\theta - \theta_c) \end{aligned} \tag{17}$$

substituting (17) into (16) gives

$$\begin{aligned} &\xi + 2a(\xi - \xi_c) + 2b(\theta - \theta_c) + \frac{\xi}{2} + a\xi \\ &+\frac{\cos\theta}{\sin\theta}c\xi(\xi - \xi_c) + \frac{\cos\theta}{\sin\theta}d\xi(\theta - \theta_c) + d\xi = 0 \end{aligned} \tag{18}$$

We need to consider two cases

Case 1

$$\begin{aligned} \theta_c \neq 0 \qquad & let \quad \xi \to \xi_c, \quad \theta \to \theta_c \\ & p = -(a + d) = 3/2 \end{aligned} \tag{19}$$

Any off–axis critical point will follow (19).

Case 2

$$\begin{aligned} \theta_c = 0, \quad c = 0 \quad & let \quad \xi \to \xi_c, \quad \theta \to \theta_c \\ & p = 3/2 + d \\ q = ad &= (p - 3/2)(3/2 - 2p) \end{aligned} \tag{20}$$

Any on–axis critical point will follow (20).

The end points of the $(p, q)$ trajectory for the on–axis critical points are determined by the boundary conditions for each flow at $\xi = 0$ and $\xi \to \infty$. For example the point $(p, q) = (\frac{7}{4}, -\frac{1}{2})$ represents the on–axis saddle point of the irrotational dipole flow induced by the momentum source. The point $(p, q) = (\frac{5}{4}, \frac{1}{4})$ represents the on–axis node of the steady Landau–Squire jet. *Thus the $(p, q)$ trajectory is predetermined and the qualitative behavior of the nonlinear problem is completely known even though a solution is not known.* Moreover the $(p, q)$ trajectory and the three states of motion described above are universal for the class of jet–like flows studied.

## V. Numerical Solution of the Round Jet

The solutions described in section II are closed form solutions of the linearized equations of motion. The discovery that these solutions contain critical behavior involving a vortex roll–up, and that this roll–up occurs without any accumulation of vorticity led us to an in–depth

study of the full nonlinear problem for the round jet to try to better understand the role that nonlinearity plays in the transition process.

A numerical solution of the full nonlinear equations of motion for the round jet has been carried out up to a Reynolds number which is high enough to fully describe the transition process. The numerical solution utilizes a two step process initialized by the linear analytic solution. The quasi–linear vorticity equation is solved with a known stream function. The calculated vorticity is used to solve Poisson's equation for an updated stream function and the process is repeated until convergence. The near field boundary condition is simply the steady solution, (Landau–Squire solution) of the axisymmetric round jet. The far field boundary condition for the stream function is an unsteady dipole. However since the mesh extends only to a finite radius ($\xi_\infty = 15$) a special boundary condition was developed which utilizes a multipole expansion of the stream function. This is used in the form of a Neumann boundary condition along with the assumption of zero vorticity at the boundary. The coefficients of this stream function multipole expression are known analytically for the dipole term and numerically for the higher order terms by use of the Biot–Savart integral of the current numerical values of vorticity. The numerical method utilizes a new direct method for solving large (up to 6400 x 6400) sparse block matrices using minimal memory. This solver can be used only on tri–block matrix systems. It involves the inversion of three transfer matrices which are only of 80x80 elements each. The original matrix diagonals are retained while the transfer matrices are computed, (throwing away the old ones as the solver works its way down the main diagonal) until the end of the diagonal is reached. Then the transfer matrices are recomputed as the solution vector is being generated while the solver works its way back up the main diagonal. This passing up and down the main diagonal while carrying only a few nonsparse matrices is the key to minimal memory usage. The computations were carried out on the CDC 7600 at NASA Ames Research Center.

The computations were first carried out on a 30x30 mesh with uniformly spaced semi-circles of constant $\xi$. A special coordinate stretcher was employed in the angular direction to pile more rays near the main axis of the jet as the Reynolds number was increased. Convergence was achieved up to a Reynolds number of 30. However, numerical instability began to dominate the solution above $Re = 21$ leading to a type of numerical vorticity clumping. When the resolution was doubled to a 60x60 mesh the instability along with the numerical "large eddies" vanished and smooth results were obtained. Figure 3 shows a comparison of computed vorticity and stream function at $Re = 30$ for the two meshes. Both meshes give identical results for $Re$ up to 15. We believe that the results on the 60x60 mesh are accurate up to about $Re = 25$ although we have not repeated these computations on a finer mesh to demonstrate mesh independence.

Figures 4, 5 and 6 show the results of the computations on the 60x60 mesh at four different Reynolds numbers. The quantities displayed are self–similar stream function, $G(\xi,\theta)$, vorticity, $W(\xi,\theta) = wt$ and particle paths, $Re^2U - \frac{\xi}{2}, Re^2\frac{V}{\xi}$. The calculations show that the critical Reynolds numbers of the nonlinear problem are lower than those determined from the linearized solution. After the first bifurcation Reynolds number, $Re_1 = 5.5$, is exceeded the angular position of the off–axis node (Figure 4b) moves rapidly (with increasing $Re$) away from the axis until $Re_2 = 7.545$ is exceeded at which point the node (now a stable focus) begins to move back toward the axis (Figures 5 and 6). As in the linear case the focus or roll–up occurs without any local accumulation of vorticity. To see this compare vorticity and particle paths in Figure 5.

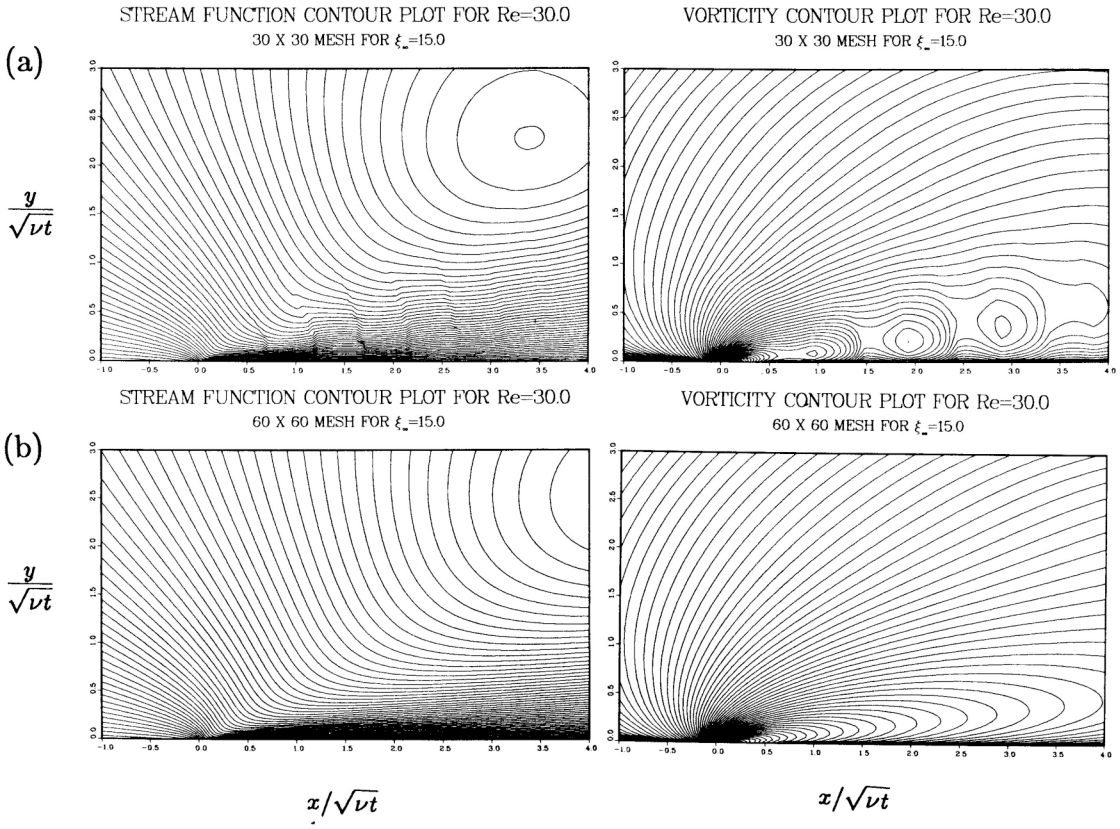


Figure 3. Computed solutions for the round jet at $Re = 30.0$ showing:
a) vorticity clumping due to numerical instability on a 30x30 mesh,
b) smooth solution on a 60x60 mesh.

## VI. Mixing of a Fluid Interface

The various solutions have been used to calculate the time evolution of a fluid interface set into motion by each of the three flows studied. The results show a number of contrasting mixing characteristics related to the Reynolds number history of each flow. Figure 7a shows results for the linearized solution of the vortex ring. At small time, the Reynolds number is large and the interface rolls rapidly. At a Reynolds number of approximately 23, the critical point in the entrainment diagram changes from a stable focus to a stable node. At this point the tendency for the interface to further roll–up terminates. As the decay process continues, mixing has essentially ceased and the interface moves slowly outward retaining its rolled–up form as vestige of its early high Reynolds number history. Figure 7c shows results for the linearized solution of the ramp jet. At small time, the Reynolds number is small and the interface distorts slowly. At a Reynolds number of approximately 8 the critical point in the entrainment diagram changes from a stable node to a stable focus and a starting vortex begins. Figure 7b shows results for three separate realizations of the round jet and illustrates interface distortion by the three states of motion shown in Figure 2. Note the peculiar corner which developes on the interface in the middle figure. Note in all cases the wide variation in total strain along the interface with maximum strain occuring on the axis. Note also the layering in total strain within the vortex roll–up associated with portions of the interface which, at $t = 0$, lay alternately to the inside or outside of the point which would later lie at the center of the roll–up.

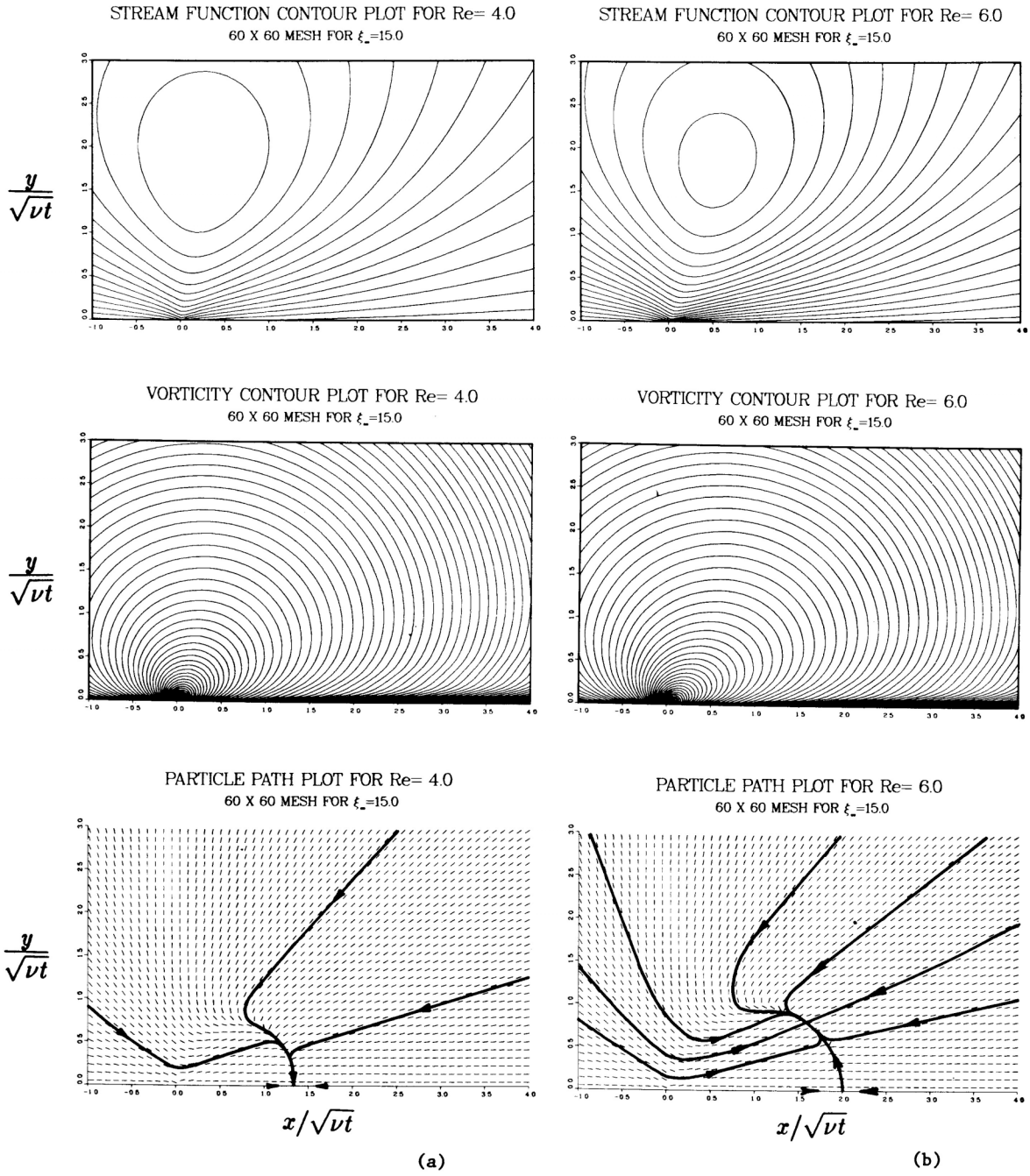


Figure 4. Computed solutions for the round jet at a) $Re = 4.0$ and b) $Re = 6.0$. Quantities displayed are self–similar stream function, vorticity and particle paths.

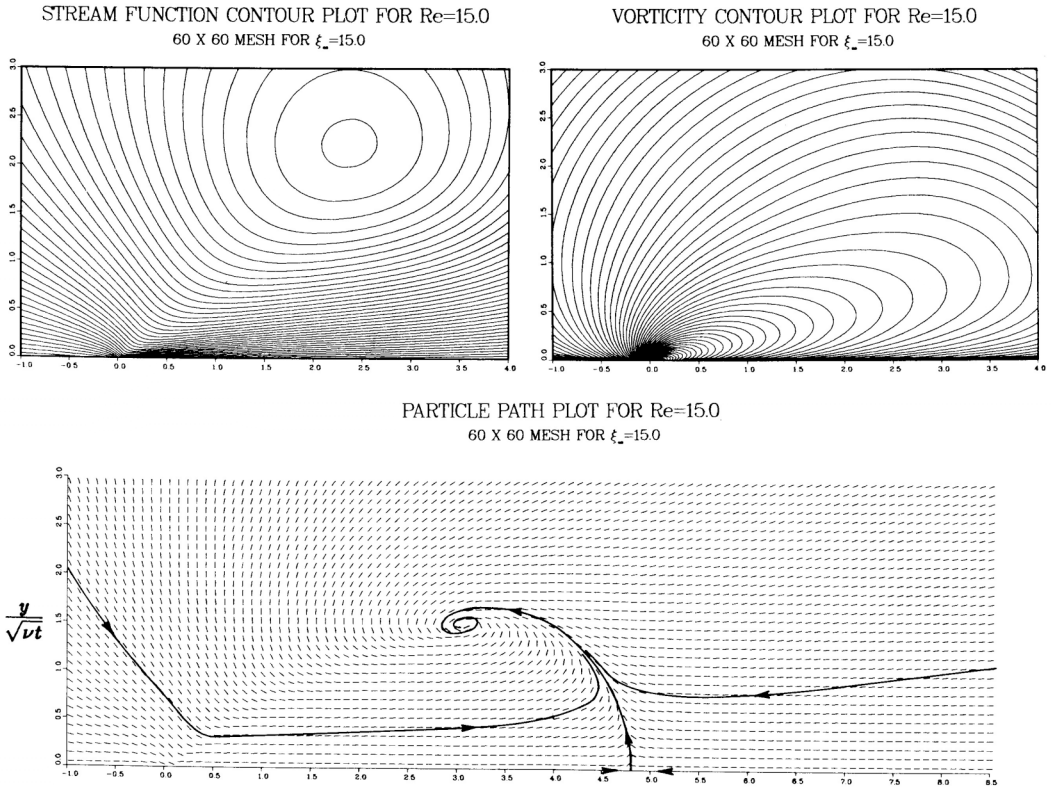


Figure 5. Computed solution for the round jet at $Re = 15.0$.

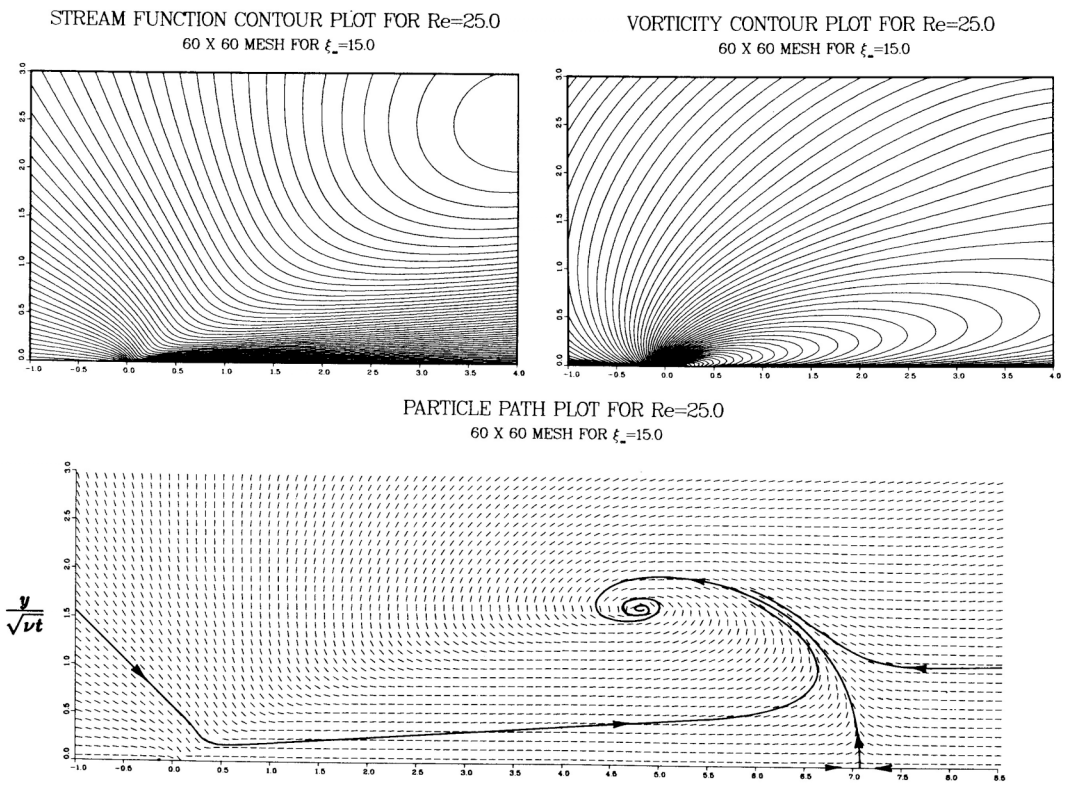


Figure 6. Computed solution for the round jet at $Re = 25.0$.

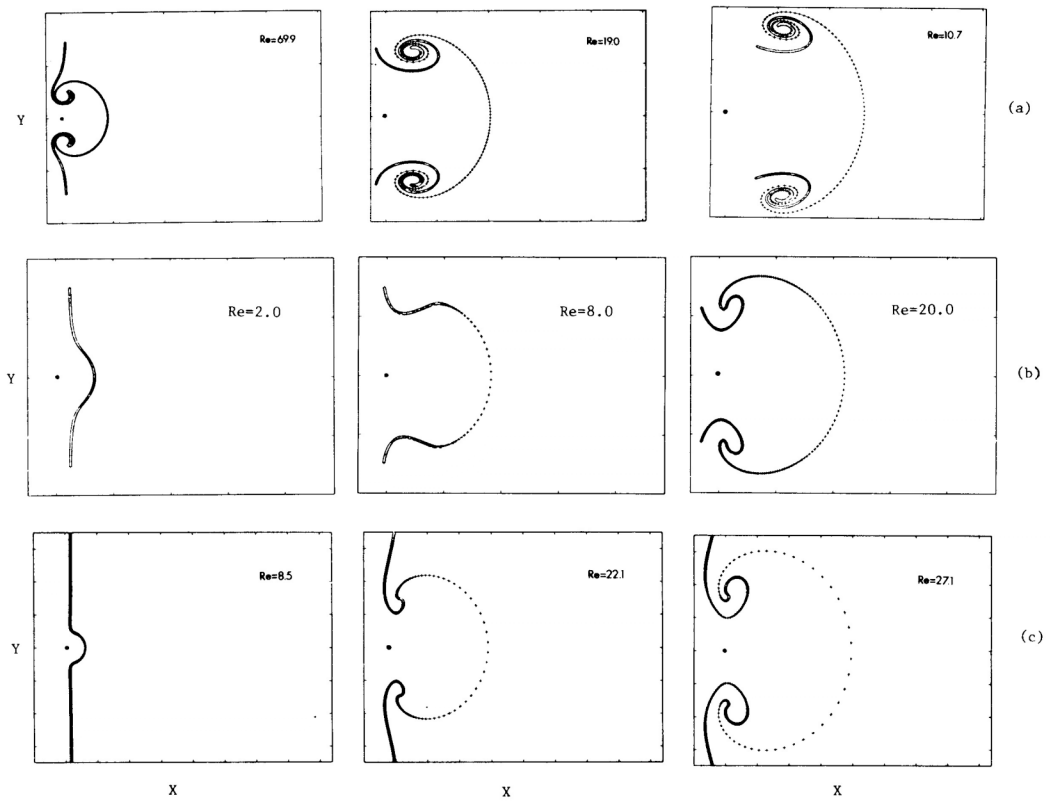


Figure 7. Distortion of a material interface by linearized solutions of: a) the vortex ring, b) the round jet (three realizations), c) the ramp jet.

A motion picture has been prepared showing the mixing of two interfaces by the three states of motion for the computed nonlinear solution of the round jet and by the linearized solutions for the vortex ring and ramp jet. The process of making the movie involved first computing the values of the steam function for a 60x60 mesh and then developing a second and third order system of splines about each node point to produce a continuous function. These splines were then marched through time using a fourth order Runge–Kutta method. Plots were generated at various time intervals, (typically at 1/24 sec.) on a CRT which was photographed frame by frame by an animator's movie camera.

## Reference

1) Cantwell, B. J. (1981) *Transition in the Axisymmetric Jet.* J. Fluid Mech., Vol. 104, pp. 369–386.

## Acknowledgment

This work was supported by NASA Ames Research Center under Grants NSG 2392 and NCC 2–21.